A semi-empirical model for free-convection condensation on horizontal pin-fin tubes

Ali, HM; Briggs, A

Abstract

A simple semi-empirical correlation accounting for the combined effect of gravity and surface tension has been developed for condensation on horizontal pin-fin tubes. The model divides the heat transfer surface into five regions, i.e. two types of pin flank, two types of pin root and the pin tip. Data for three fluids (i.e. steam, ethylene glycol and R113) condensing on eleven tubes with different geometries were used in a minimization process to find three empirical constants in the final expression. The model gives good overall agreement (within ± 20 %) with the experimental data, as well as correctly predicting the dependence of heat-transfer enhancement on the various geometric parameters and fluid types.

Key Words

Condensation; pin-fin tube; semi-empirical correlation; heat transfer enhancement; phase change.

A Semi-Empirical Model for Free-Convection Condensation on Horizontal Pin-Fin Tubes

Hafiz Muhammad Ali [a] and Adrian Briggs [b]

[a] Department of Mechanical Engineering, University of Engineering and Technology, Taxila 47050, Pakistan

[b] School of Engineering and Materials Science, Queen Mary University of London, Mile End Road, London E1 4NS, UK

1. Introduction

A significant number of experimental investigations have been reported on free-convection condensation heat-transfer on horizontal integral-fin tubes; see for example [1-11]. During the condensation process, liquid retained on the lower part of tube insulatesthe fin flanks and root from heat transfer, This condensate retention on integral-fin tubes was first observed by Katz et al. [12] and afterwards experimentally investigated by many other investigators for a wide range of fluid and tube combinations [1, 3, 13, 14,15]. The development of an analytical correlation to predict this condensate retention angle (measured from the top of the tube up to the point where whole fin flanks become flooded with condensate) was a pivotal step for the development of a theoretical heat-transfer model for condensation on integral-fin tubes. Such an analytical correlation to predict condensate retention angle on integral-fin tube was first reported by Honda et al. [1] (later developed by Owen et al. [16] and Rudy and Webb [13]) to accomplish the requirement, the following expression was produced for retention angle, $\emptyset_f$, measured from the top of the tube,

$$\emptyset_f = \cos^{-1}\left[\left(\frac{2\sigma\cos\theta}{\rho g s R_o}\right) - 1\right] for\ s < 2h \qquad (1)$$

Reliable and simple heat-transfer models for integral-fin tubes (i.e. Honda and Nozu [17], Rose [18] and Briggs and Rose [19]) accounting for the combined effects of surface tension and gravity on heat-transfer were later developed which are now readily available for design engineers. With the help of above experimental and theoretical work, optimal tube geometries are now identified for a wide range of working fluids condensing on integral-fin tubes.

In the recent past, attention has been focused on more complex pin-fin tubes (a schematic of three dimensional pin-fin tube with condensate retention angle is shown in Figure 1). Many experimental investigations on pin-fin tubes (Sukathme et al. [20], Briggs [21], Baiser and Briggs [22], Ali and Briggs [23, 24 and 25]) have shown their superior heat transfer performance (up to 25%) over the equivalent integral-fin tubes (i.e. with the same fin height, root diameter and longitudinal pin thickness and spacing). When Briggs [22] tested steam, four out of six pin-fin tubes were fully flooded with condensate i.e. the only available area for heat transfer wasthe pin tips. When compared with equivalent integral-fin tubesthese fully flooded tubes gave about 20% more heat transfer, despite the fact that available area was only about half of the equivalent integral-fin tube. Qin et al. [26] tested R134a condensing on two pin-fin tubes of different geometries, one made of copper and another made of stainless steel. Heat transfer enhancements were found to be 7.9 and 3.3 for copper and stainless steel pin-fin tubes respectively. The superior performance of copper was due to its longer pin height and high thermal conductivity.

In order to exploit the superior experimental performance of pin-fin tubes, it is necessary to develop a heat-transfer model to optimize these tubes to discover their full potential. For the development of an accurate heat-transfer model for pin-fin tubes, the development of a predictive correlation of condensate retention angles on pin-fin tubes was the start point which was recently proposed by Ali and Briggs [27] as following equation;

$$\emptyset_f = \cos^{-1}\left[\left(1 - C \times \frac{s_c}{t_c}\right)\left(\frac{2\sigma}{\rho g s R_o}\right) - 1\right] \quad for\ s < 2h \qquad (2)$$

Equation 2 was found to give agreement within 15% with experimental retention angle data on pin-fin tubes reported by the authors and also by other investigators [13, 14, and 20] for a wide range of fluid and tube combinations.

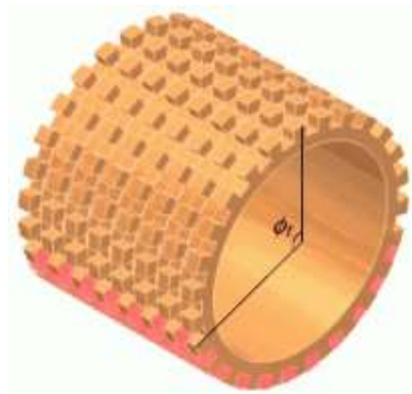

Figure 1 Schematic of Three-Dimensional Pin-Fin Tube

Kumar et al. [28] proposed a generalized empirical model to predict the vapour-side, heat-transfer coefficient on integral-fin and pin-fin tubes (the only theoretical model so far proposed for condensation on pin-fin tubes). They proposed that the heat-transfer coefficient was a function of fluid properties, tube geometry and condensate mass flow rate.They claimed agreement to within±15% with their own experimental data for one tube for steam and one for R-134a, respectively. Cavallini et al. [29] and Namasivayam [30] reported the poor performance of this model for copper integral-fin tubes. Later, Ali and Briggs [23] when compared this model with experimental data of pin-fin tubes, it showed poor agreement with most of the data. One possible reason for the inadequate performance of the model might be neglect of condensate retention on the lower part of the tubes. In addition, the model is based on the assumption of a linear pressure gradient along the pin or fin flank which has been shown to give poor results for integral-fin tubes (see Briggs and Rose [31]).

More recently, Kundu and Lee [32] reported optimized profiles for vertical fins of variable cross section subjected to condensation of saturated vapour under free convection, while Kundu [33] and Kundu and Ghosh [34] extended the analysis to horizontal circular pins under free and forced convection condensation respectively. These included the conjugate effects of conduction in the pins. The choice of fin profiles, however, meant that surface tension effects could be neglected and the condensation process was modeled assuming gravity drainage alone (in 32 and 33) and gravity plus vapour shear (in 34).

Finally, Nagarani et al. [35] presented a detailed review covering a wide range of extended surfaces applications in heat transfer problems, including condensation on pin-fin tubes.

In the present work, a simple and reliable semi-empirical model to predict vapour-side, heat-transfer enhancement ratio for condensation on horizontal pin-fin tubes has been developed. The proposed model is based on an approach adopted in the models of Rose [18] and Briggs and Rose [19] for condensation on horizontal integral-fin tubes.These authors modeled the effects of gravity using the approach of Nusselt [36] and surface tension using dimensional analysis. The model is validated in the light of earlier data for condensation on copper pin-fin tubes.

2. Development of a Semi-Empirical Model for Condensation on Horizontal Pin-Fin Tubes

2.1 Generalized Equations for Condensation Heat-Transfer Accounting for the Effects of Gravity and Surface Tension

The approach of Nusselt [36] for gravity drained condensation on flat plates and horizontal tube, along with dimensional analysis for the effects of surface tension, suggests the following general expressions for heat flux,

For an arbitrary flat surface at angle Ø to the vertical,

$$q_L = \left\{\frac{\rho h_{fg} k^3 \Delta T^3}{\mu}\left(\frac{A_L \tilde{\rho} g \cos \emptyset}{x_L} + \frac{B\sigma}{x_\sigma^3}\right)\right\}^{1/4} \tag{3}$$

where, x_L = linear dimension of plate length, A_L= 0.943^4 as suggested by Nusselt [36] theory for a vertical plate and B is a constant for surface tension driven flow.

For a horizontal tube,

$$q_d = \left\{\frac{\rho h_{fg} k^3 \Delta T^3}{\mu}\left(\frac{A_D \tilde{\rho} g}{x_D} + \frac{B\sigma}{x_\sigma^3}\right)\right\}^{1/4} \tag{4}$$

where, x_D = linear dimension of tube diameter, A_D= 0.728^4 as suggested by Nusselt [36] theory for a horizontal whole tube . For the case of an integral-fin or pin-fin tube, where the lower part of tube retains condensate, this value can be adjusted as A_D=$\{\xi(\emptyset_f)\}^3$. $\xi(\emptyset_f)$for the appropriate flooding angle was approximated by Rose [18] as,

$$\xi(\emptyset_f) = 0.874 + 0.1991\times10^{-2}\emptyset_f - 0.2642\times10^{-1}{\emptyset_f}^2 + 0.5530\times10^{-2}{\emptyset_f}^3 - 0.1363\times10^{-2}{\emptyset_f}^4 \tag{5}$$

where, $\emptyset_f$ is the flooding angle and for pin-fin tubes is calculated using equation 2.

It should be noted that x_σ appears in the denominators of equations 3 and 4 and so a decreasing$x_\sigma$will have a positive effect on heat flux. In addition, since surface tension effects will be most significant at the edges of the surfaces, where there are sharp changes in condensate surface curvature, surfaces with larger perimeters and smaller areas would be expected to have higher average heat fluxes. For these reasons, in equations 3 and 4, x_σ is here set equal to the ratio of area to perimeter for the appropriate condensing surface i.e. $x_\sigma = A/P$.

Expressions for Condensation Heat-Transfer Rate on Pin-Fin Tube

In this section, equations 3 and 4 are applied to the appropriate regions of the pin-fin tube to find separate expressions for the heat-transfer rate to these regions. Figure 2 identifies five regionson the pin-fin tubes for heat-transfer i.e. pin tip, pin flank 1, pin flank 2, pin root 1 and pin root 2. This division of pin-fin tube into five distinctive regions is necessary due to the very different geometrical configurations of the five regions; in particular their orientation with respect to gravity and to the expected differences in the effect of surface tension forces. For the pin tip where there is no condensate flooding, all pin tips are considered active for heat transfer around the tube. For pin flanks and pin roots, there will be heat transfer only in the unflooded regions of the tube i.e. through pin flanks and pin roots not blanked by retained condensate.

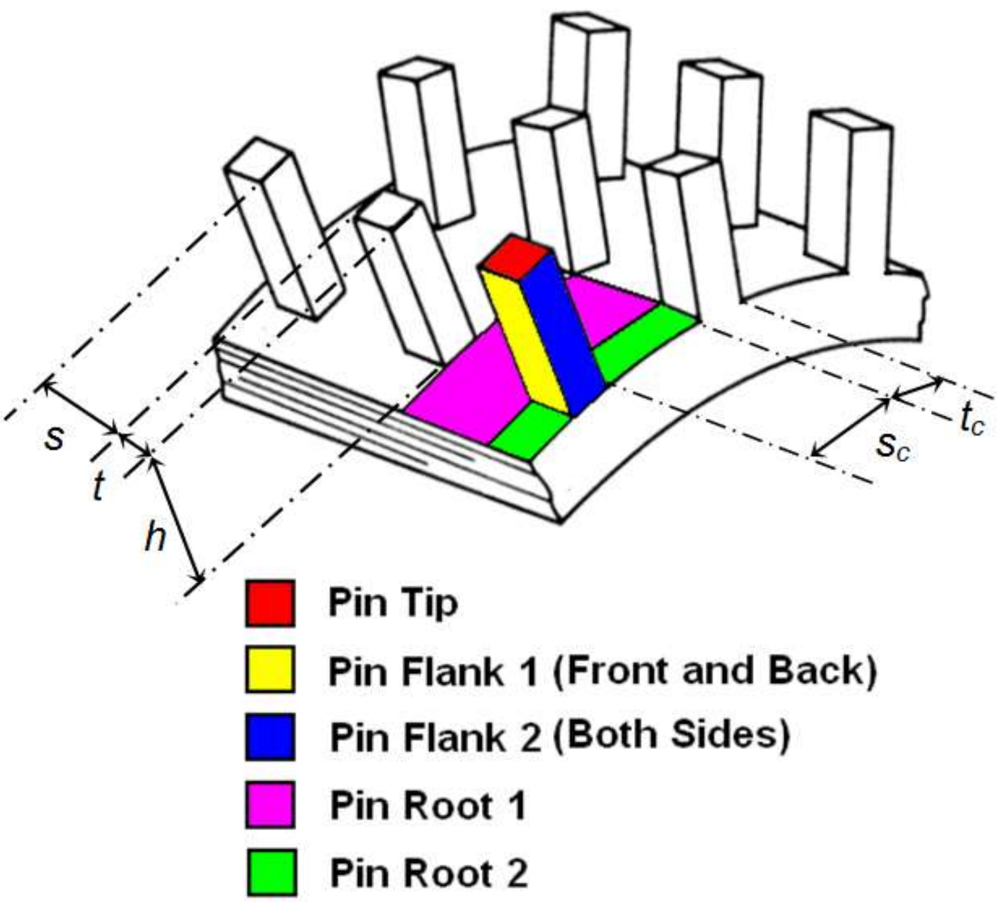

Figure 2 Schematic of Pin-Fin Tube Identifying Five Regions for Heat-Transfer

<u>Pin Tip</u>

For a pin $\boldsymbol{i}$ making an angle ϕ to the vertical axis as shown in Figure 3, a pin tip with a longitudinal thickness of t and circumferential thickness of t_c can be treated as a flat plate. Applying equation 3 with $A_L = 0.943^4$, $x_L = t_c$ and $x_\sigma = A_{tip}/P_{tip}$, the heat flux can be written as,

$$q_{tip,i} = \left[\frac{\rho h_{fg} k^3 \Delta T^3}{\mu}\left\{\frac{0.943^4 \tilde{\rho} g \sin \emptyset}{t_c} + \frac{B_{tip}\sigma}{\left(A_{tip}/P_{tip}\right)^3}\right\}\right]^{1/4} \quad (6)$$

where B_{tip} is an empirical constant and A_{tip}/P_{tip} is the area to perimeter ratio for the pin tip as follows,

$$\frac{A_{tip}}{P_{tip}} = \frac{t_c t}{2(t_c + t)} \quad (7)$$

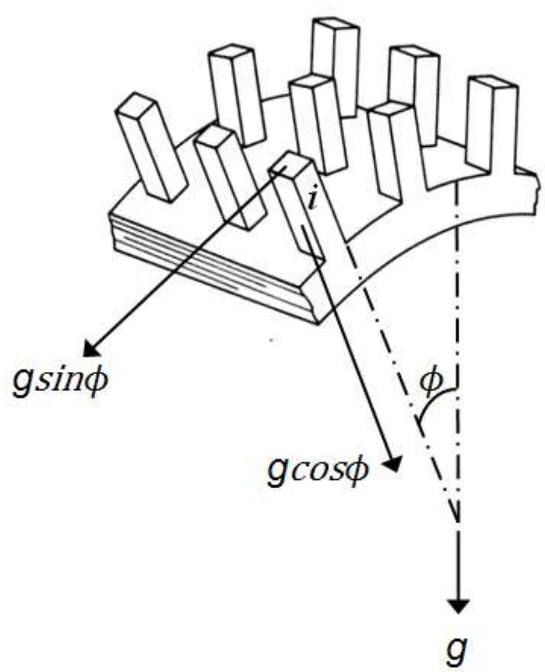

Figure 3 Physical Model of Pin-Fin Tube

When the total number of pins per circumference is *n*, ϕ for the *i*th pin (counting from the top) can be given as,

$$\emptyset = \frac{i}{n/2}\pi \quad (8)$$

Substituting equation 7 into equation 6 and multiplying by the pin-tip area givesthe heat-transfer rate for pin tip i. Finally, the total heat-transfer rate for all the pin tips around the circumference can be obtained as,

$$Q_{tip} = 2\sum_{i=1}^{n/2} t_c t \left[\frac{\rho h_{fg} k^3 \Delta T^3}{\mu}\left\{\frac{0.943^4 \tilde{\rho} g \sin \emptyset}{t_c} + \frac{B_{tip}\sigma}{\left(\frac{t_c t}{2(t_c+t)}\right)^3}\right\}\right]^{1/4} \quad (9)$$

<u>Pin Flank 1</u>

For pin flank 1 (see Figure 2) with a longitudinal thickness t and height h, making an angle ϕ with the vertical plane as shown in Figure 3, equation 3 with $A_L = 0.943^4$, $x_L = h$ and $x_\sigma = A_{flank\ 1}/P_{flank\ 1}$, becomes,

$$q_{flank\ 1,i} = \left[\frac{\rho h_{fg} k^3 \Delta T^3}{\mu}\left\{\frac{0.943^4 \tilde{\rho} g |\cos \emptyset|}{h} + \frac{B_{flank\ 1}\sigma}{\left(A_{flank\ 1}/P_{flank\ 1}\right)^3}\right\}\right]^{1/4} \quad (10)$$

Where $B_{flank\ 1}$is an empirical constant and $A_{flank\ 1}/P_{flank\ 1}$ is the area to perimeter ratio for pin flank 1 given as,

$$\frac{A_{flank\ 1}}{P_{flank\ 1}} = \frac{ht}{2(t+h)} \quad (11)$$

Substituting equation 11 into equation 10 and multiplying by area, the following expression gives the total heat-transfer rate for all pin flanks 1,

$$Q_{flank\ 1} = 4\sum_{i=1}^{j/2} ht \left[\frac{\rho h_{fg} k^3 \Delta T^3}{\mu}\left\{\frac{0.943^4 \tilde{\rho} g |\cos \emptyset|}{h} + \frac{B_{flank\ 1}\sigma}{\left(\frac{ht}{2(t+h)}\right)^3}\right\}\right]^{1/4} \quad (12)$$

Here ***j*** is the total number of pins above the flooding point, since those below this point will be insulated to heat transfer by the retained condensate. ***j*** can be calculated as follows,

$$j = n\frac{\emptyset_f}{\pi} \tag{13}$$

<u>Pin Flank 2</u>

Applying equation 3 to pin flank 2 (see Figure 2) with $A_L = 0.943^4$, $x_L = h_v$ and $x_\sigma = A_{flank\ 2}/P_{flank\ 2}$ gives,

$$q_{flank\ 2,i} = \left[\frac{\rho h_{fg} k^3 \Delta T^3}{\mu}\left\{\frac{0.943^4 \tilde{\rho} g}{h_v} + \frac{B_{flank\ 2}\sigma}{\left(A_{flank\ 2}/P_{flank\ 2}\right)^3}\right\}\right]^{1/4} \tag{14}$$

where $B_{flank\ 2}$ is an empirical constant and $A_{flank\ 2}/P_{flank\ 2}$ is the area to perimeter ratio for pin flank 2, given as,

$$\frac{A_{flank\ 2}}{P_{flank\ 2}} = \frac{ht_c}{2(t_c + h)} \tag{15}$$

h_v in equation 14 is a mean vertical pin height (see Figure 4) for a pin making angle ϕ with the vertical axis, and is given by,

$$h_v = \frac{ht_c}{\left|\sqrt{h^2 + {t_c}^2}\sin(\emptyset + \beta)\right|} \tag{16}$$

where,

$$\beta = \tan^{-1}(t_c/h) \tag{17}$$

Substituting equations15 and 16 into equation 14 and multiplying by the area,the total heat-transfer rate for all pin flanks 2 is given by,

$$Q_{flank\,2} = 4\sum_{i=1}^{j/2} ht_c \left[\frac{\rho h_{fg} k^3 \Delta T^3}{\mu}\left\{\frac{0.943^4 \tilde{\rho} g}{\frac{ht_c}{\left|\sqrt{h^2+t_c{}^2}\sin(\emptyset+\beta)\right|}} + \frac{B_{flank\,2}\sigma}{\left(\frac{ht_c}{2(t_c+h)}\right)^3}\right\}\right]^{1/4} \qquad (18)$$

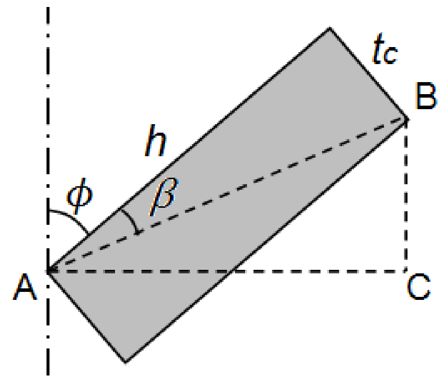

$$h_v = \frac{Area}{AC} = \frac{ht_c}{|AB\sin(\emptyset+\beta)|} = \frac{ht_c}{\left|\sqrt{h^2+t_c{}^2}\sin(\emptyset+\beta)\right|}$$

Where, $\beta = \tan^{-1}(t_c/h)$

Figure 4 Expressions for Mean Vertical Pin Height

<u>Pin Root 1</u>

Pin root 1 can be treated as a horizontal plain tube with the inclusion of condensate flooding on the lower part of tube as in Rose [18]. Applying equation 4 with$A_D = \{\xi(\emptyset_f)\}^3$, $x_D = d$ and $x_\sigma = A_{root\,1}/P_{root\,1}$, gives the following expression for heat flux,

$$q_{root\ 1} = \left\{ \frac{\rho h_{fg} k^3 \Delta T^3}{\mu} \left(\frac{\left\{\xi\left(\emptyset_f\right)\right\}^3 \tilde{\rho} g}{d} + \frac{B_{root\ 1}\sigma}{(A_{root\ 1}/P_{root\ 1})^3} \right) \right\}^{1/4} \tag{19}$$

where, $\xi\left(\emptyset_f\right)$ can be calculated using equation 5, $B_{root\ 1}$ is an empiricalconstant and $A_{root\ 1}/P_{root\ 1}$ is area to perimeter ratio for pin flank 1 and can be approximated as,

$$\frac{A_{root\ 1}}{P_{root\ 1}} = \frac{\emptyset_f ds}{2t_c j} \tag{20}$$

where, s is longitudinal pin spacing and $j$is calculated using equation 13. Substituting equation 20 into equation 19 and multiplying by the area, the total heat-transfer rate can be given by,

$$Q_{root\ 1} = \emptyset_f ds \left\{ \frac{\rho h_{fg} k^3 \Delta T^3}{\mu} \left(\frac{\left\{\xi\left(\emptyset_f\right)\right\}^3 \tilde{\rho} g}{d} + \frac{B_{root\ 1}\sigma}{\left(\frac{\emptyset_f ds}{2t_c j}\right)^3} \right) \right\}^{1/4} \tag{21}$$

<u>Pin Root 2</u>

Since the circumferential pin spacing is usually quite small compared to the circumference of the tube, pin root 2 can be approximated to a flat plate. By applying equation 3 with $A_L = 0.943^4$, $x_L = s_c$ and $x_\sigma = A_{root\ 2}/P_{root\ 2}$, the expression for the heat flux for a pin root 2 can be written as,

$$q_{root\ 2,i} = \left[\frac{\rho h_{fg} k^3 \Delta T^3}{\mu} \left\{ \frac{0.943^4 \tilde{\rho} g \sin\emptyset}{s_c} + \frac{B_{root\ 2}\sigma}{(A_{root\ 2}/P_{root\ 2})^3} \right\} \right]^{1/4} \tag{22}$$

where, $B_{root\,2}$ is an empirical constant, s_c is the circumferential pin spacing, ϕ can be calculated using equation 15 and $A_{root\,2}/P_{root\,2}$ is the area to perimeter ratio for pin root 2 given by,

$$\frac{A_{root\,2}}{P_{root\,2}} = \frac{s_c t}{2t} = \frac{s_c}{2} \tag{23}$$

Substituting equation 23 into equation 22 and multiplying by the area of pin root 2 gives the following expression for the total heat-transfer rate to pin root 2,

$$Q_{root\,2} = 2\sum_{i=1}^{j/2} s_c t \left[\frac{\rho h_{fg} k^3 \Delta T^3}{\mu}\left\{\frac{0.943^4 \tilde{\rho} g \sin \emptyset}{s_c} + \frac{B_{root\,2}\sigma}{\left(\frac{s_c}{2}\right)^3}\right\}\right]^{1/4} \tag{24}$$

2.2 Vapour-Side, Heat-Transfer Enhancement Ratio

The total heat-transfer rate through a pin-fin tube for one longitudinal pin pitch can be computed as a sum of the heat-transfer rates to the pin tips, pin flanks and inter-pin roots. The vapour-side, heat-transfer enhancement ratio of the pin-fin tube at constant temperature difference, defined as the total heat-transfer rate to one longitudinal pin pitch of the pin-fin tube, divided by the heat-transfer rate to a plain tube of length equal to longitudinal pin pitch and diameter equal to the pin root diameter (which can be found from the Nusselt [36] theory of free-convection condensation on horizontal plain tubes) can be given by,

$$\varepsilon_{\Delta T} = \frac{Q_{tip} + Q_{flank\,1} + Q_{flank\,2} + Q_{root\,1} + Q_{root\,2}}{\pi d(t+s)\left\{0.728\left(\frac{\rho\tilde{\rho} g h_{fg} k^3 \Delta T^3}{\mu d}\right)\right\}} \tag{25}$$

Substituting equations 9, 12, 18, 21 and 24 into equation 25, the final expression for the vapour-side, heat-transfer enhancement ratio for a rectangular pin-fin tube can be written as,

$$\varepsilon_{\Delta T}=\frac{2t_c t}{0.728\pi d(s+t)}\sum_{i=1}^{n/2}\left[\left\{0.943^4\sin\emptyset\frac{d}{t_c}+B_{tip}\frac{d}{\left(\frac{t_c t}{2(t_c+t)}\right)^3}\frac{\sigma}{\tilde{\rho}g}\right\}\right]^{1/4}$$

$$+\frac{4ht}{0.728\pi d(s+t)}\sum_{i=1}^{j/2}\left[\left\{0.943^4|\cos\emptyset|\frac{d}{h}+B_{flank1}\frac{d}{\left(\frac{ht}{2(h+t)}\right)^3}\frac{\sigma}{\tilde{\rho}g}\right\}\right]^{1/4}$$

$$+\frac{4ht_c}{0.728\pi d(s+t)}\sum_{i=1}^{j/2}\left[\left\{0.943^4\frac{d}{\frac{ht_c}{\left|\sqrt{h^2+t_c{}^2}\sin(\emptyset+\beta)\right|}}+B_{flank\,2}\frac{d}{\left(\frac{ht_c}{2(t_c+h)}\right)^3}\frac{\sigma}{\tilde{\rho}g}\right\}\right]^{1/4}$$

$$+\frac{\emptyset_f s}{0.728\pi(s+t)}\left[\left\{\left\{\xi\left(\emptyset_f\right)\right\}^3+B_{root\,1}\frac{d}{\left(\frac{\emptyset_f ds}{2t_c j}\right)^3}\frac{\sigma}{\tilde{\rho}g}\right\}\right]^{1/4}$$

$$+\frac{2s_c t}{0.728\pi(s+t)}\sum_{i=1}^{j/2}\left[\left\{0.943^4\sin\emptyset\frac{d}{s_c}+B_{root\,2}\frac{d}{\left(\frac{s_c}{2}\right)^3}\frac{\sigma}{\tilde{\rho}g}\right\}\right]^{1/4} \qquad (26)$$

In equation 26, $\emptyset$ and β can be calculated using equations 8 and 17 and j can be found from equation 13. Only two thermophysical properties are involved in the expression of enhancement ratio i.e. surface tension, σ, and condensate density, ρ.

Determination of the Unknown Constants

Equation 26 contains 5 empirical constants B_{tip}, B_{flank1}, $B_{flank\,2}$, $B_{root\,1}$ and $B_{root\,2}$ which need to be evaluated using experimental data. To make the case simple, the unknown constants for pin flanks (i.e. pin flank 1 and pin flank 2) and for tube roots (i.e. root 1 and root 2) were assumed to be the same i.e. $B_{flank1}=B_{flank2}=B_{flank}$ and $B_{root\,1}=B_{root\,2}=B_{root}$. These three unknown constants, B_{tip},B_{flank} and B_{root} were then found using a least square fit method by minimizing the sum of squares of relative residuals in the vapour-side, heat-transfer enhancement ratios.

For the minimization process, the experimental data used are taken from the investigations of (Briggs [21], Baiser and Briggs [22] and Ali and Briggs [23, 24 and 25]) on copper pin-fin tubes covering a range of data for 3 different condensing fluids (steam, ethylene glycol and R-113) and 11 pin-fin tube geometries. As in the model, the vapour-side, enhancement ratios are defined as the heat flux of the pin-fin tube divided by that of a plain tube with diameter equal to the pin root diameter and at the same vapour-side temperature difference.

Table 1 gives the values of the three unknown constants, found by minimization of sum of squares of relative residuals of the vapour-side enhancement ratios, which gave the best fit of equation 26 to the data. A relative standard deviation was found to be 15.5 %.

Table 1 Empirical Constants

B_{tip}	B_{flank}	B_{root}	Std_{rel} *
0.02	0.001	0.01	15.49 %

* Relative standard deviation

The larger value of B_{tip} may be justified in the light of experimental data of steam reported by Briggs [21] who found significant enhancement ratios for fully flooded tubes, indicating that surface tension effects dominate on small pin tips where the sharp changes in surface curvature cause significant localized thinning the condensate layer.

The experimental values of vapour-side, heat-transfer enhancement ratios for all tube and fluid combinations used in the best fit process are listed in Table 2. Surface tension in equation 26 was calculated at saturation temperature of 470 K, 373 K and 320 K for ethylene glycol, steam and R-113 respectively, whereas condensate density was calculated at a reference temperature equal to the vapour temperature minus $2\Delta T/3$, where ΔT is the average vapour-side temperature difference of the experimental data, taken as 100 K, 20 K and 21 K for ethylene glycol, steam and R-113 respectively. Since the model neglects temperature drop along the pins the data used in the fitting process were restricted to those for copper tubes, where the effects of none uniform pin surface temperature would be expected to be negligible (See Briggs and Rose [19] for evidence that this is the case for integral-fin tubes.)

Table 2 Heat-Transfer Enhancement Ratios

	R-113 [22, 23, 24, 25]		Ethylene Glycol [23, 24, 25]		Steam [21, 22]	
Tubes	$(\varepsilon_{\Delta T})_{calc}$	$(\varepsilon_{\Delta T})_{obs}$	$(\varepsilon_{\Delta T})_{calc}$	$(\varepsilon_{\Delta T})_{obs}$	$(\varepsilon_{\Delta T})_{calc}$	$(\varepsilon_{\Delta T})_{obs}$
P1	3.59	3.34	3.58	2.86	3.19	2.59
P2	4.92	4.77	4.62	4.19	4.28	2.91
P3	5.34	5.83	4.31	4.08	2.22	2.34
P4	8.11	8.32	6.3	5.41	2.47	2.80
P5	5.81	6.51	5.03	4.06	2.11	2.47
P6	8.43	9.16	6.92	5.77	2.37	2.61
P7	5.46	5.92	5.29	4.91	4.74	3.86
P8	4.48	4.47	4.24	3.89	4.04	3.59
P10	4.81	5.77	4.45	4.89	4.05	4.41
P11	3.94	4.05	4.02	4.17	3.56	4.50
P12	3.36	3.99	3.3	3.50	3.1	3.98

3. Comparison of Semi-Empirical Expression with Experimental Data

Figure 5 gives a global comparison of the model with the available experimental data on copper pin-fin tubes. It can be seen that equation 26 predicts nearly all the data to within ± 20 %.

Figures 6a and 6b compares theory and experimental data plotted as dependence of enhancement ratio on circumferential pin spacing, for t_c = 0.5 mm and t_c = 1.0 mm respectively. For both fluids i.e. R-113 and ethylene glycol, equation 26 shows good agreement with experimental data and predicts an increase in enhancement ratio with decreasing circumferential spacing suggesting that a smaller circumferential pin spacing i.e. less than the smallest tested (0.5 mm) may produce even higher heat-transfer enhancements for both fluids and circumferential pin thicknesses. Figures 7a and 7b shows a similar pair of plots to Figures 6a and 6b, theory over predicts enhancement ratios at t_c = 0.5 mm (Figure 7a) and under predicts at t_c = 1.0 mm (Figure 7b). This could be due to the fact that the model does not account for temperature drop along the pins, which for condensation of steam, where vapour-side, heat-transfer coefficients are high, could be significant and lead to a decrease in decrease in “pin efficiency”at the lower pin thickness.

Figures 8 and 9 show the variation of enhancement ratio with pin height. The experimental data show a reasonable agreement with the theory in all cases and predict the same dependence on height and fluid. Better agreement with theory is seen for R-113. For steam and the highest pin height (Figure 8a) theory over predicts data by about 40 %, possibly for the same reason as explained above.

Figures 10a and 10b give dependence of enhancement ratio on circumferential pin thickness for ethylene glycol and pin heights of 0.9 mm and 1.6 mm respectively while Figures 9c and 9d plot enhancement ratio against circumferential pin thickness for circumferential pin spacings of 0.5 mm and 1.0 mm. For all cases, the theory predicts the data reasonably well, however, better agreementis found at larger circumferential pin thickness.

Figures 11a and 11b compare the theory with experimental data of R-113 and steam with enhancement ratio plotted as a function of circumferential pin thickness at pin heights of 0.9 mm and 1.6 mm. Values and overall trends are again in very good agreement.

4. Conclusion

A semi-empirical correlation based on the approach used in the models of Rose [18] and Briggs and Rose [19] to account for the combined effect of gravity and surface tension has been developed for condensation on horizontal pin-fin tubes (i.e. equation 26). Important results are given below;

- The model predicts experimental data, covering enhancement ratios in a range from 2.5 to 9.2, for three fluids (i.e. steam, ethylene glycol and R113) and eleven tubes of different geometries, to within ± 20 % (see Figure 5).

- Detailed comparison between the model and experimental data indicate that the model satisfactorily predicts the dependence of heat transfer enhancement on both geometric variables and fluids. This suggests the model could be used to optimize tube geometries for given applications. Such an optimization exercise would be complex, given that the model includes six independent geometric variables. Recent work [e.g. 37-39] however suggests possible approaches for such optimization procedures.

- The comparisons with data for condensation of steam suggest that where heat-transfer coefficients are high, "fin efficiency" effects due to significant temperature variation along the pins can lead to significant error in the model [see 40, 41]. For these cases, and where the low thermal conductivity tube materials are used, it is suggested that a conjugate model be developed, possibly along the lines of [19 or 32-34].

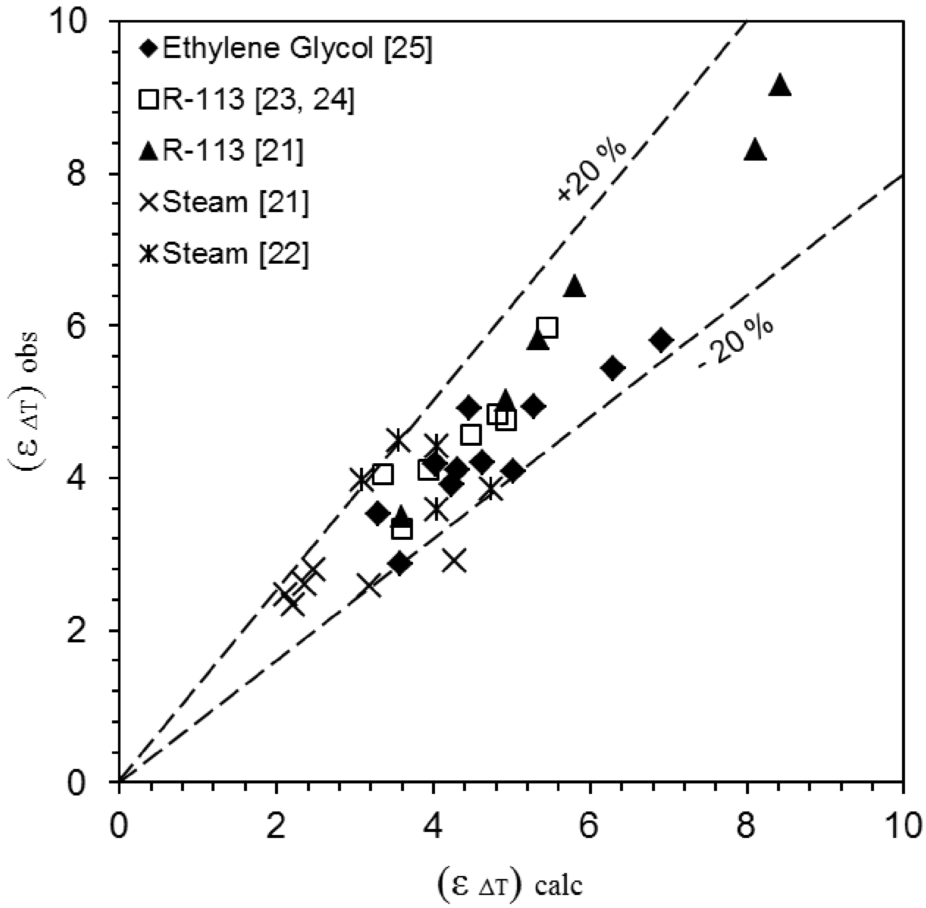

Figure 5 Comparison of Available Experimental Data with Eqn. 26

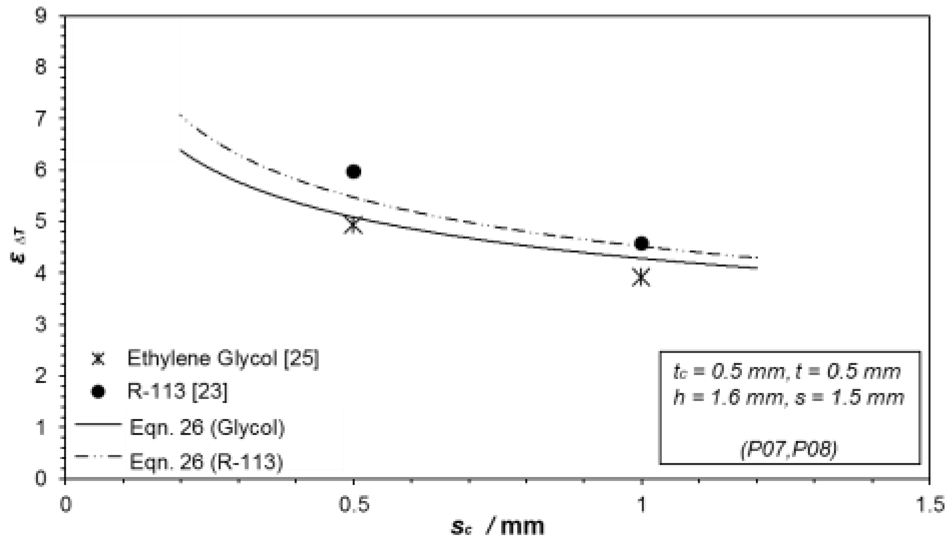

(a) t_c = 0.5 mm

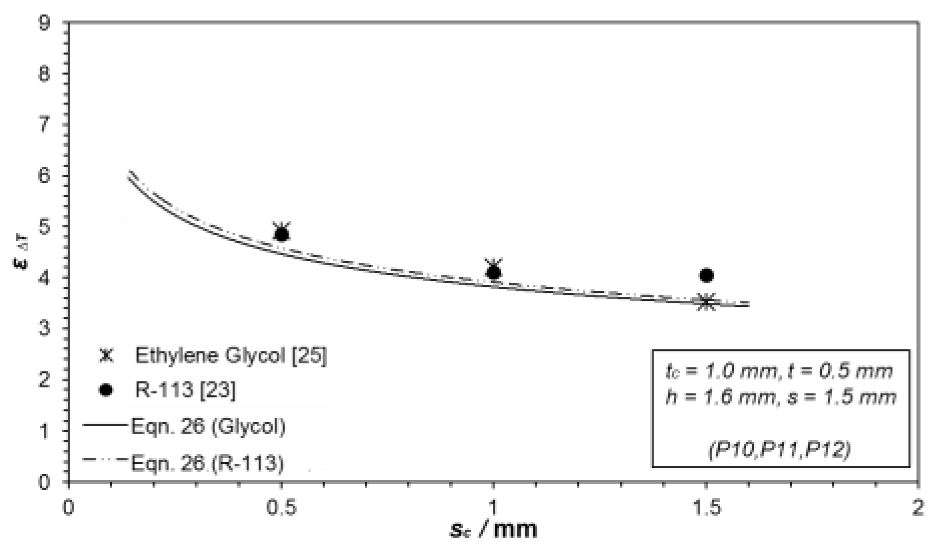

(b) t_c= 1.0 mm

Figure 6 Variation of Heat-Transfer Enhancement Ratio with Circumferential Pin Spacing (Comparison of Experimental Data of Ali and Briggs [23, 25] with Current Model)

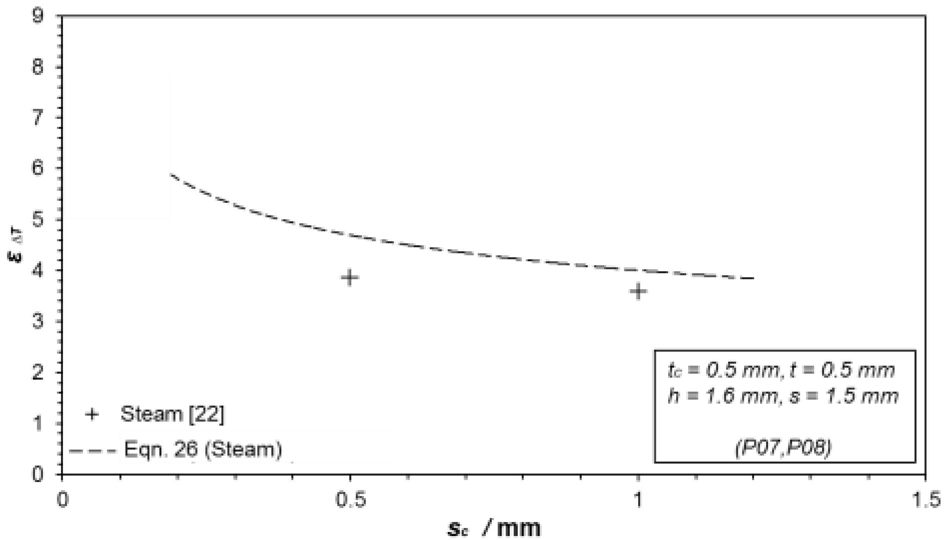

(a) $t_c = 0.5$ mm

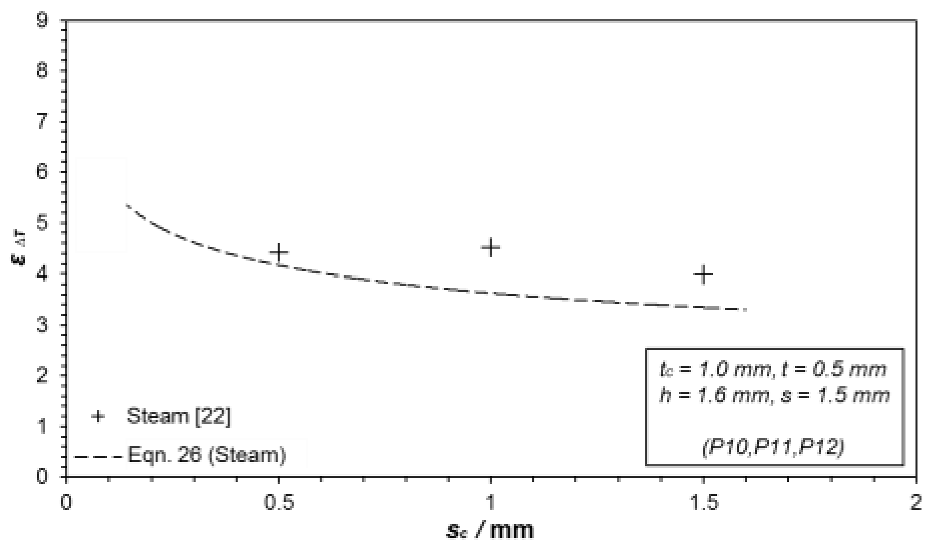

(b) $t_c = 1.0$ mm

Figure 7 Variation of Heat-Transfer Enhancement Ratio with Circumferential Pin Spacing (Comparison of Experimental Data of Baiser and Briggs [22] with Current Model)

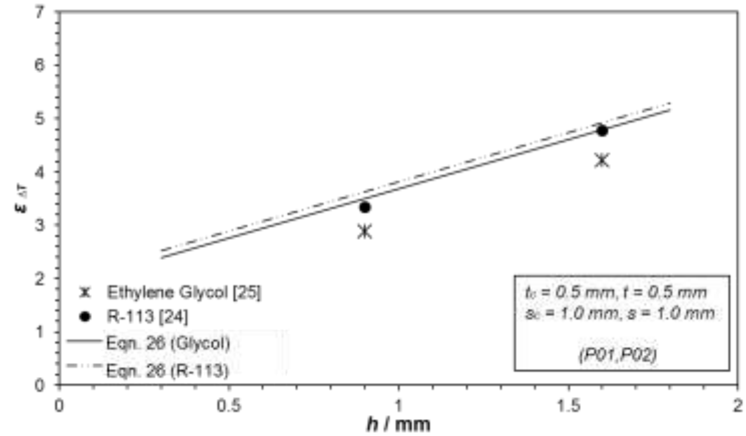

(a)

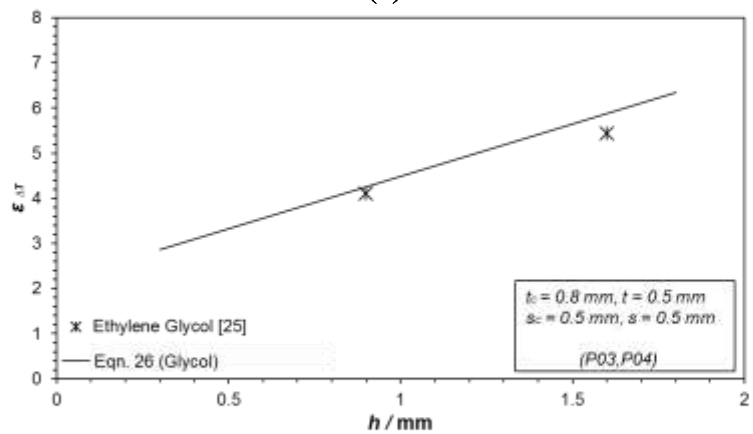

(b)

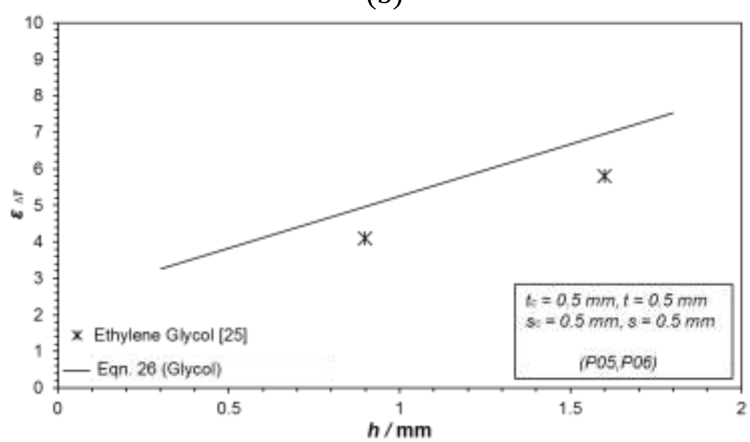

(c)

Figure 8 Variation of $\varepsilon_{\Delta T}$ with Pin Height
(Comparison of Experimental Data of Ali and Briggs [24, 25] with Current Model)

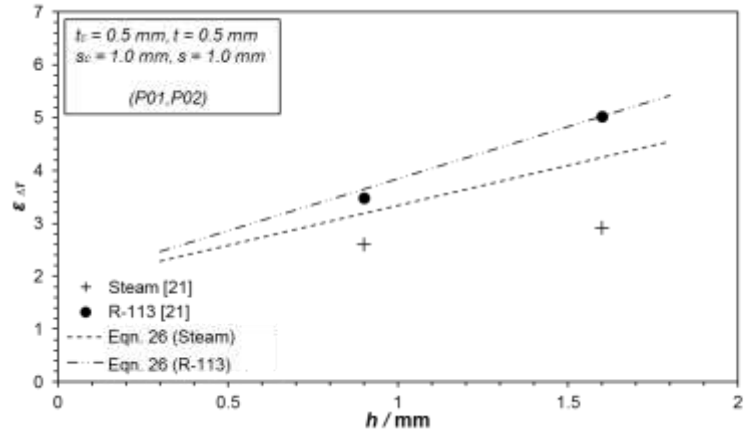

(a)

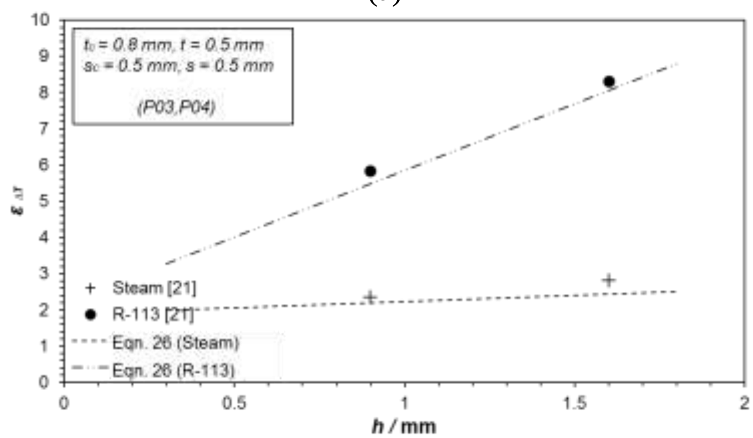

(b)

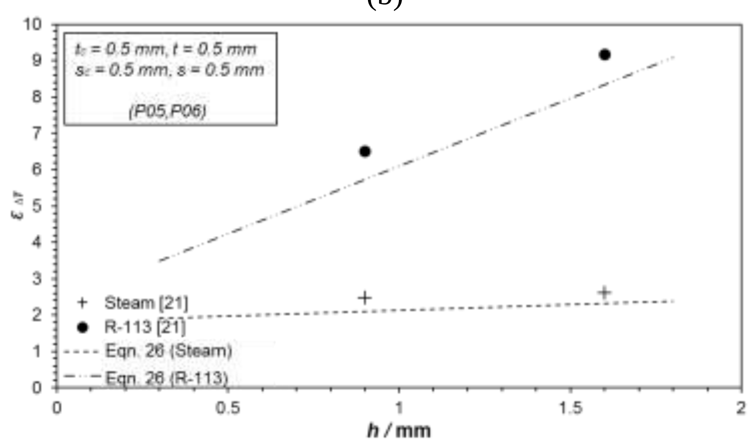

(c)

Figure 9 Variation of $\varepsilon_{\Delta T}$ with Pin Height
(Comparison of Experimental Data of Briggs [21] with Current Model)

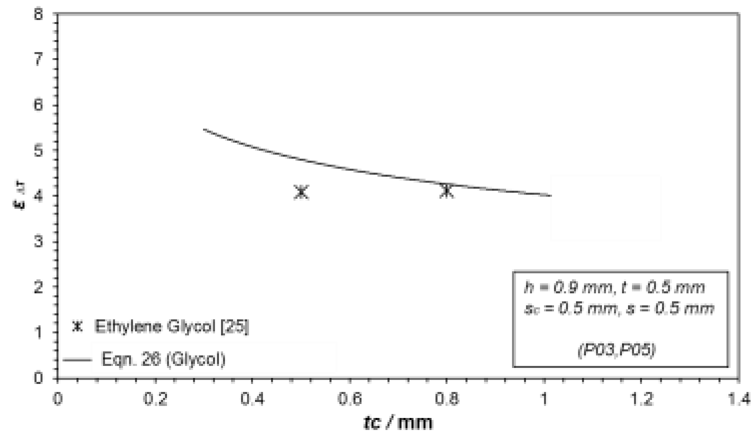

(a) h = 0.9 mm

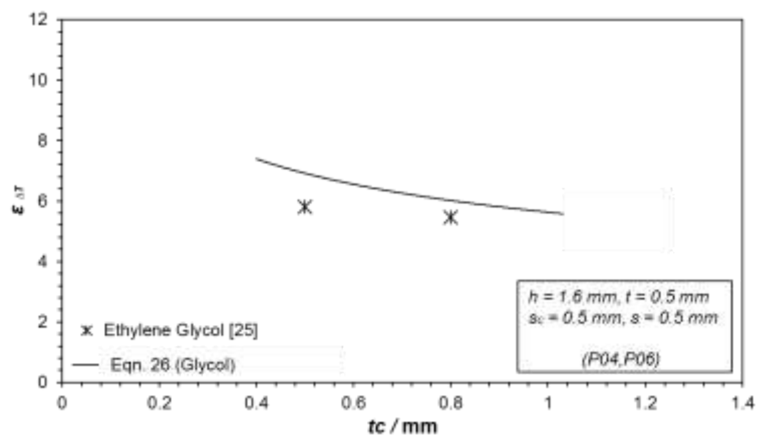

(b) h = 1.6 mm

Figure 10 Variation of Heat-Transfer Enhancement Ratio with Circumferential Pin Thickness (Comparison of Experimental Data of Ali and Briggs [25] with Current Model)

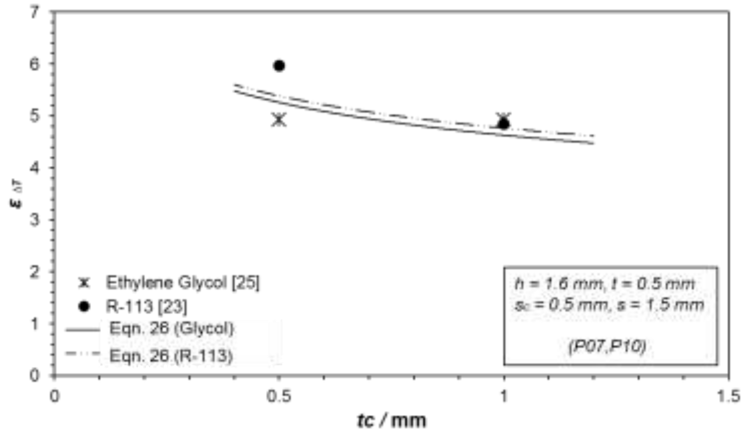

(c) s_c = 0.5 mm

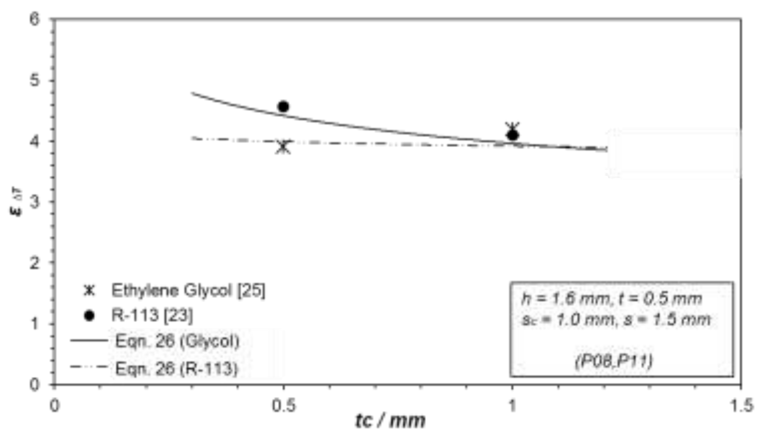

(d) s_c = 1.0 mm

Figure 10 (Continued)

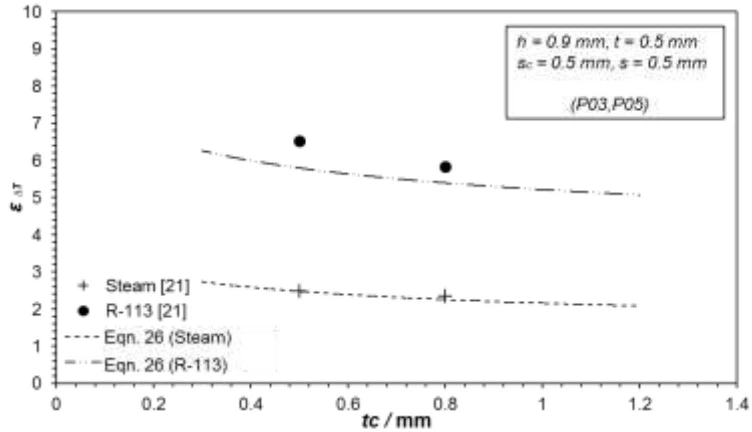

(a) h = 0.9 mm

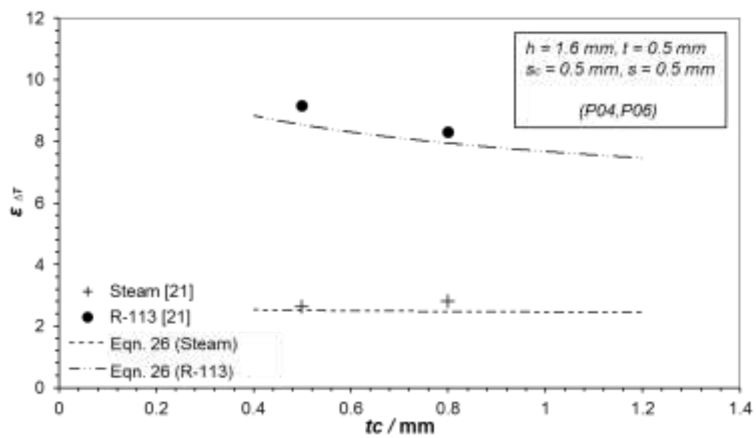

(b) h = 1.6 mm

Figure 11 Variation of Heat-Transfer Enhancement Ratio with Circumferential Pin Thickness
(Comparison of Experimental Data of Briggs [21] with Current Model)

Nomenclature

A	area
A_D	constant in Eqn. (4)
$A_{flank\,1}$	area of pin flank 1
$A_{flank\,2}$	area of pin flank 2
A_L	constant in Eqn. (3)
$A_{root\,1}$	area of root 1
$A_{root\,2}$	area of root 2
A_{tip}	area of pin tip
B	constant in Eqn. (3)
B_{flank}	empirical constant for pin flank
$B_{flank\,1}$	empirical constant for pin flank 1
$B_{flank\,2}$	empirical constant for pin flank 2
B_{root}	empirical constant for root
$B_{root\,1}$	empirical constant for root 1
$B_{root\,2}$	empirical constant for root 2
B_{tip}	empirical constant for pin tip
C	constant in Eqn. (2)
d	outside diameter of plain tube or fin or pin root diameter of finned or pinned tube
d_o	fin or pin tip diameter of fin or pin tube
g	specific force of gravity
j	number of pins in unflooded region
h	fin or pin height
h_{fg}	specific enthalpy of vaporization
h_v	mean vertical fin or pin height
k	thermal conductivity of condensate
L	length of flat plate
n	total number of pins per circumference
P	perimeter
$P_{flank\,1}$	perimeter of pin flank 1

$P_{flank\ 2}$ perimeter of pin flank 2

$P_{root\ 1}$ perimeter of root 1

$P_{root\ 2}$ perimeter of root 2

P_{tip} perimeter of pin tip

$Q_{flank\ 1}$ heat-transfer rate through all pin flanks 1

$Q_{flank\ 2}$ heat-transfer rate through all pin flanks 2

$Q_{root\ 1}$ heat-transfer rate through root 1

$Q_{root\ 2}$ heat-transfer rate through root 1

Q_{tip} heat-transfer rate through all pin tips

q_d heat flux on outside of a horizontal tube defined by Eqn. (4)

q_{flank} heat flux to fin flank in unflooded part of tube

$q_{flank\ 1,i}$ heat flux to flank 1 for pin *i* defined by Eqn. (10)

$q_{flank\ 2,i}$ heat flux to flank 2 for pin i defined by Eqn. (14)

q_L heat flux on a plate defined by Eqn. (3)

$q_{root\ 1}$ heat flux through root 1 defined by Eqn. (19)

$q_{root\ 2,i}$ heat flux to pin root 2 for a pin *i* defined by Eqn. (22)

q_{tip} heat flux to fin tip

$q_{tip,i}$ heat flux to pin tip *i* defined by Eqn. (6)

$q_{tip,flood}$ heat flux to fin tip in flooded part of tube

R_o pin tip radius

s fin spacing at fin root or longitudinal pin spacing at pin root

s_c circumferential pin spacing

t fin tip thickness or longitudinal pin tip thickness

t_c circumferential pin thickness

x_D linear dimension of tube diameter

x_L linear dimension of plate length

x_σ characteristic length for surface tension driven flow in model

Greek Letters

β	angle defined by Eqn. (17)
ΔT	temperature difference across the condensate film
$\varepsilon_{\Delta T}$	vapour-side, heat-transfer enhancement ratio, heat flux for finned or pinned tube based on fin or pin root diameter divided by heat flux for smooth tube with same fin/pin root diameter, at same vapour-side, temperature difference
μ	dynamic viscosity of condensate
$\xi(\emptyset)$	function given by Eqn. (5)
ρ	density of condensate
ρ_v	density of vapour
$\tilde{\rho}$	$\rho - \rho_v$
σ	surface tension
θ	half angle at fin tip
$\emptyset$	angle measured from the top of a fin or pin tube
$\emptyset_f$	condensate flooding or retention angle measured from the top of a fin or pin tube

Subscripts

calc	calculated
obs	experimental
rel	pertaining to relative residuals
Std	pertaining to standard deviation

References

1. Honda, H., Nozu S. and Mitsumori, K., (1983), Augmentation of Condensation on Finned Tubes by Attaching a Porous Drainage Plate, Proc. ASME-JSME Thermal Engineering Joint Conf., Vol. 3, 289-295.
2. Yau, K. K., Cooper, J. R., and Rose, J. W., (1985), Effect of Fin Spacing on the Performance of Horizontal Integral-Fin Condenser Tubes, Trans. ASME J. Heat Transfer, Vol. 107, 377-383.

3. Yau, K. K., Cooper, J. R., and Rose, J. W., (1986), Horizontal Plain and Low-Finned Condenser Tubes- Effect of Fin Spacing and Drainage Strips on Heat Transfer and Condensate Retention, Trans. ASME J. Heat Transfer, Vol. 108, 946-950.
4. Masuda, H. and Rose, J.W., (1985), An Experimental Study of Condensation of R-113 on Low Integral-Fin Tubes, Proc. Int. Symposium on Heat Transfer., 2, Paper No. 32.
5. Masuda, H. and Rose, J.W., (1988), Condensation of Ethylene Glycol on Horizontal Finned Tubes, Trans. ASME J. Heat Transfer, Vol. 110, 1019-1022.
6. Wanniarachchi, A. S., Marto, P. J. and Rose, J. W., (1986), Film Condensation of Steam on Horizontal Finned Tubes: Effect of Fin Spacing, Trans. ASME J. Heat Transfer, Vol. 108, 960-966.
7. Marto, P. J., Mitrou, E., Wanniarachchi, A. S., and Rose, J. W., (1986), Film Condensation of Steam on Horizontal Finned Tubes: Effect of Fin Shape, Proc. 8th International Heat Transfer Conference, Vol. 4, 1695-1700.
8. Marto, P. J., Zebrowski, D., Wanniarachchi, A. S. and Rose, J. W., (1990), An Experimental Study of R-113 Film Condensation on Horizontal Integral Fin Tubes, Trans. ASME J. Heat Transfer, Vol. 112, 759-767.
9. Briggs, A. Wen, X. L. and Rose, J. W., (1992), Accurate Heat Transfer Measurements for Condensation on Horizontal, Integral-Fin Tubes, Trans. ASME J. Heat Transfer, Vol. 114, 719-726.
10. Briggs, A., Huang, X. S. and Rose, J. W., (1995), An Experimental Investigation of Condensation on Integral Fin Tubes: Effect of Fin Thickness, Height and Thermal Conductivity, Proc. ASME Nat. Heat Transfer Conference, HTD, Vol. 308, 21-29.
11. Park, K. J. and Jung, D., (2008), Optimum Fin Density of Low Fin Tubes for the Condensers of Building Chillers with HCFC123, J. of Energy Conservation and Management, Vol. 49, 2090-2094.
12. Katz, D. L., Hope, R. E., and Datsko, S. C., (1946), Liquid Retention on Finned Tubes, Dept. of Eng. Res., Univ. of Michigan, project M592.
13. Rudy, T. M., and Webb, R. L., (1985), An Analytical Model to Predict Condensate Retention on Horizontal Integral Fin Tubes, Trans. ASME J. Heat Transfer, Vol. 107, 361-368.
14. Briggs, A., (2005) Liquid Retention on Three-Dimensional Pin-Fin Tubes, 2nd Int. Exergy, Energy and Environment Symp., Kos, Paper No. IEEES2-171.

15. Fitzgerald, C. L., Briggs, A., Rose, J. W., and Wang, H. S., (2012), Effect of Vapour Velocity on Condensate Retention between Fins during Condensation on Low-Finned Tubes, International J.of Heat and Mass Transfer, Vol. 55, 1412–1418.
16. Owen, R. G., Sardesai, R. G., Smith, R. A. and Lee, W. C., (1983), Gravity Controlled Condensation on Low Integral Fin Tubes, in Condenser: Theory and Practice, I. Chem. E. Symposium, Serial No. 75, 415–428.
17. Honda, H. and Nozu S., (1987), A Prediction Method for Heat Transfer During Film Condensation on Horizontal Low Integral Fin Tubes, Trans. ASME J. Heat Transfer, Vol. 109, 218–225.
18. Rose, J. W., (1994), An Approximate Equation for the Vapour-side Heat Transfer Coefficient for Condensation on Low Finned Tubes, International J. of Heat andMass Transfer, Vol. 37, 865–875.
19. Briggs, A. and Rose, J. W., (1994), Effect of Fin Efficiency on a Model for Condensation Heat Transfer on a Horizontal Integral Fin Tube, International J.of Heat and Mass Transfer, Vol. 37, 457–463.
20. Sukhatme, S. P., Jagadish, B. S. and Prabhakaran, P., (1990), Film Condensation of R-11 Vapor on Single Horizontal Enhanced Condenser Tubes, Trans. ASME J. of Heat Transfer, Vol. 112, 229–234.
21. Briggs, A., (2003), Enhanced Condensation of R-113 and Steam on Three-Dimensional Pin-Fin Tubes, Exp. Heat Transfer, Vol. 16, 61–79.
22. Baiser, M., and Briggs, A., (2009), Condensation of Steam on Pin-Fin Tubes: Effect of Circumferential Pin Thickness and Spacing, J. of Heat Transfer Eng., Vol. 30, 1017–1023.
23. Ali, H. M. and Briggs, A., (2012), Condensation of R-113 on Pin-Fin Tubes: Effect of Circumferential Pin Thickness and Spacing, J. of Heat Transfer Eng., Vol. 33, 205–212.
24. Ali, H. M. and Briggs, A., (2013), Condensation Heat Transfer on Pin-Fin Tubes: Effect of Thermal Conductivity and Pin Height, J. of Applied Thermal Engineering, Vol. 60, 465–471.
25. Ali, H. M. and Briggs, A., (2012), Enhanced Condensation of ethylene glycol on Pin-Fin Tubes: Effect of Pin Geometry, Trans. ASME J. of Heat Transfer, Vol. 134, 011503.

26. Qin, P., Zhang, Z., Xu, T., Gao, X. and Wang, S., (2013), Experimental Investigation on Condensation Heat Transfer of R134a on Single Horizontal Copper and Stainless Steel Three-Dimensional Finned Tubes, AIP Conf. Proc., 1547, 513.
27. Ali, H. M. and Briggs, A. (2014), An investigation of Condensate Retention on Pin-Fin Tubes, J. of Applied Thermal Engineering, Vol. 63 (2), 503-510.
28. Kumar, R., Varma, H. K., Mohanty, B. and Agrawal, K. N., (2002), Prediction of Heat Transfer Coefficient During Condensation of Water and R-134a on Single Horizontal Integral-Fin Tubes, International Journal of Refrigeration, Vol. 25, 111–126.
29. Cavallini, A., Cesni, G., Del Col, D., Doretti, L., Longo, G. A., Rossetto, L. and Zilio, C., (2003), Condensation Inside and Outside Smooth and Enhanced Tubes: A Review of Recent Research, Int. J. Refrigeration, Vol. 26, 373-392.
30. Namasivayam, S., (2006), Condensation on Single Horizontal Integral-Fin Tubes: Effect of Vapour Velocity and Fin Geometry, PhD Thesis, Univ. of London.
31. Briggs, A., and Rose, J.W., (1995), Models for Condensation Heat Transfer on Low-Finned Tubes, Proc. 2nd Baltic Heat Transfer Conf., Riga, 215–225.
32. Kundu, B. and Lee, K-S., (2011), Optimum Configurations of Vertical Fins under Condensation of Saturated Vapor, International Journal of Refrigeration, Vol. 34, 1048–1056.
33. Kundu, B., (2009), Approximate Analytical Method for Prediction of Performance and Optimum Dimensions of Pin Fins subject to Condensation of Quiescent Vapor, International Journal of Refrigeration, Vol. 32, 1657–1671.
34. Kundu, B., and Ghosh, G., (2009), An Approximate Analytical Prediction about Thermal Performance and Optimum Design of Pin Fins subject to Condensation of Saturated Steam Flowing under Forced Convection, International Journal of Refrigeration, Vol. 32, 809–825.
35. Nagarani, N., Mayilsamy, K., Murugesan, A. and Kumar, G. S., (2014), Review of Utilization of Extended Surfaces in Heat Transfer Problems, Renewable and Sustainable Energy Reviews, Vol. 29, 604–613.
36. Nusselt, W., (1916), Die Oblerflachenkondensation des Wasserdampfes, Z. Vereines Deutsch. Ing., Vol. 60, 541-546, 569-575.

37. Hajmohammadi, M. R., Poozesh, S., Nourazar, S. S. and Manesh, A. H., (2013), Optimal architecture of heat generating pieces in a fin, Journal of Mechanical Science and Technology, Vol. 27, 1143-1149.

38. Hajmohammadi, M. R., Poozesh, S. And Nourazar, S. S., (2012), Constructal design of multiple heat sources in a square-shaped fin, Journal of Process Mechanical Engineering, Vol. 226, 324-336.

39. Hajmohammadi, M. R., Rahmani, M., Campo, M. A. and Shariatzadeh, J. O., (2014), Optimal design of unequal heat flux elements for optimized heat transfer inside a rectangular duct, Energy, Vol. 68, 609-616.

40. Hajmohammadi, M. R. and Nourazar S. S., (2014), Conjugate forced convection heat transfer from a heated flat plate of finite thickness and temperature-dependent thermal conductivity, Heat Transfer Engineering, Vol. 35, 863–874.

41. Hajmohammadi, M. R., Shariatzadeh, J. O., Moulod, M. and Campo, M. A., (2014), Effect of a thick plate on the excess temperature of iso-heat flux heat sources cooled by laminar forced convection flow; Conjugate analysis, Numerical Heat Transfer, Part A Vol. 66, 205–216.